Non-Fossil Origin Explains the Large Seasonal Variation of Highly Processed Organic Aerosol in the Northeastern Tibetan Plateau (3,200 m a.s.l.)

Ni, Haiyan; Yao, Peng; Zhu, Chongshu; Qu, Yao; Tian, Jie; Ma, Yongyong; Yang, Lu; Zhong, Haobin; Huang, Ru Jin; Dusek, Ulrike

Published in:
Geophysical research letters

DOI:
10.1029/2023GL104710

Geophysical Research Letters

RESEARCH LETTER
10.1029/2023GL104710

Non-Fossil Origin Explains the Large Seasonal Variation of Highly Processed Organic Aerosol in the Northeastern Tibetan Plateau (3,200 m a.s.l.)

Haiyan Ni[1,2], Peng Yao[2], Chongshu Zhu[1], Yao Qu[1], Jie Tian[1], Yongyong Ma[3], Lu Yang[1], Haobin Zhong[1,4], Ru-Jin Huang[1,5,6], and Ulrike Dusek[2]

[1]State Key Laboratory of Loess and Quaternary Geology, Key Laboratory of Aerosol Chemistry and Physics, CAS Center for Excellence in Quaternary Science and Global Change, Institute of Earth Environment, Chinese Academy of Sciences, Xi'an, China, [2]Centre for Isotope Research (CIO), Energy and Sustainability Research Institute Groningen (ESRIG), University of Groningen, Groningen, the Netherlands, [3]Meteorological Institute of Shaanxi Province, Xi'an, China, [4]School of Advanced Materials Engineering, Jiaxing Nanhu University, Jiaxing, China, [5]University of Chinese Academy of Sciences, Beijing, China, [6]Institute of Global Environmental Change, Xi'an Jiaotong University, Xi'an, China

Key Points:

- High seasonality of elemental carbon (EC) and organic carbon (OC) concentrations in the northeastern Tibetan Plateau (TP) was driven by non-fossil sources
- In the monsoon season, low EC and OC concentrations reflected local sources, with most evident contributions from fossil sources
- OC in the northeastern TP was highly atmospherically processed and thus less volatile compared to OC near sources or in urban areas

Supporting Information:

Supporting Information may be found in the online version of this article.

Correspondence to:

R.-J. Huang and U. Dusek,
huang@ieecas.cn;
u.dusek@rug.nl

Citation:

Ni, H., Yao, P., Zhu, C., Qu, Y., Tian, J., Ma, Y., et al. (2023). Non-fossil origin explains the large seasonal variation of highly processed organic aerosol in the northeastern Tibetan Plateau (3,200 m a.s.l.). *Geophysical Research Letters*, *50*, e2023GL104710. https://doi.org/10.1029/2023GL104710

Received 25 MAY 2023
Accepted 13 JUN 2023

Abstract Carbonaceous aerosol plays an important role in climate, but its sources and atmospheric processes are least understood in the Tibetan Plateau (TP), a remote yet climatically sensitive region. This study presents the first seasonal cycle of radiocarbon and stable isotope ^{13}C of organic and elemental carbon (OC and EC) in the atmosphere of the northeastern TP. Large seasonal variations of EC and OC concentrations were explained by non-fossil sources. Regardless of the season, fossil contribution to OC was strongly correlated with inverse OC concentrations. This allowed the separating a constant background source and a source responsible for OC variability that was mostly of non-fossil origin. The ^{13}C signature of OC shows that OC was highly atmospherically processed and thus less volatile than OC found near sources or in urban areas. The ^{13}C-depleted secondary sources contributed strongly to more volatile OC, whereas the ^{13}C-enriched less volatile OC suggests the influence of atmospheric aging.

Plain Language Summary The climate effects of carbonaceous aerosols (CAs) are highly uncertain and debated. The high-altitude Tibetan Plateau (TP) is sensitive to climate change, however, sources and atmospheric processes of CAs in the TP are poorly known. This is particularly challenging for organic aerosols, due to the large number of species involved in their formation and transformation processes in the atmosphere. In recent years, dual-carbon isotope characterization (i.e., radiocarbon ^{14}C and the stable carbon isotope ^{13}C) has become a promising tool to elucidate the sources and formation processes of organic aerosols. With this approach, we found that organic aerosols in the northeastern TP (Qinghai Lake) are highly atmospheric processed, and their seasonal variability is driven by a variable largely non-fossil source. Findings from this study lead to a better understanding of the sources and formation mechanisms of organic aerosols in different seasons, and thus organic aerosols' effects on climate change.

1. Introduction

Carbonaceous aerosols (CAs) are a significant and increasing fraction of the aerosol mass. They have detrimental effects on human health and exert highly uncertain impacts on regional and global climate (Bond et al., 2013; Gustafsson & Ramanathan, 2016; Kanakidou et al., 2005). However, our scientific assessments of these effects are hampered by poorly constrained sources and formation mechanisms. This is notoriously difficult for organic aerosol, because it comprises a large number of organic compounds with different physical-chemical properties (e.g., volatilities, oxidation states, etc.), and complex formation and transformation processes in the atmosphere (Fuzzi et al., 2006). In contrast, elemental carbon (EC, from incomplete combustion) aerosols are graphite-like and inert in the atmosphere.

In recent years, dual-carbon isotope characterization (i.e., radiocarbon ^{14}C and the stable carbon isotope ^{13}C) has become increasingly important for quantitatively constraining sources as well as for a better understanding of the formation processes of CAs (Dasari et al., 2019; Xu et al., 2021; Zimnoch et al., 2020). This technique relies on different ^{14}C source signatures of fossil fuel (^{14}C-free) and non-fossil sources (e.g., biomass burning), as well as different ^{13}C signatures of different classes of fossil fuel (e.g., liquid fossil fuel and coal; Andersson

et al., 2015; Winiger et al., 2017, 2019). The ability to separate coal combustion from other fossil fuel sources for EC makes ^{13}C analysis particularly valuable in China, where residential coal combustion is an important pollution source. Furthermore, the ^{13}C of organic aerosols is modified by atmospheric processes via kinetic isotope effects. Usually, secondary OC (SOC) formation from the oxidation of VOCs precursors is expected to result in a depleted ^{13}C signature, whereas atmospheric aging releases isotopically lighter carbon (e.g., CO_2, CO) leading to a gradual ^{13}C enrichment in the remaining aerosol. Analysis of ^{13}C in OC thus can give new insight into the formation and transformation processing of organic aerosols (Aggarwal & Kawamura, 2009; Li et al., 2018; Wang et al., 2010). This has inspired ^{13}C studies on sub-fractions of organic aerosols, for example, more and less volatile OC, that show indications of various atmospheric processes (Masalaite et al., 2017, 2020; Ni et al., 2022). While CAs are widely characterized in urban and rural China, sources and formation mechanisms in the pristine and climatically sensitive region of Tibetan Plateau (TP) remain less understood, especially in studies applying dual-carbon isotopic analysis.

The TP (27°–45°N, 70°–105°E) stands 5 km high over a region of ∼3 million km^2, and is one of the most remote and pristine regions in the world with little industry and sparse population. The high-altitude TP is sensitive to climate change, for example, large areas of glaciers in the TP have retreated in recent decades; the magnitude of climate warming over the TP is greater than the Northern Hemisphere and the globe (Kuang & Jiao, 2016). Despite CAs' important role in climate, their sources and atmospheric processes are least understood in the TP. To date, observation-based isotopic studies on sources and formation of CAs (particularly organic aerosols) in the TP are scarce and rarely extend over more than one season (Li, Bosch, et al., 2022; Li, Zhang, et al., 2022). In this study, we present a 1-yr study combining radiocarbon and stable carbon isotope analysis of OC and EC in the vastly understudied northeastern TP (Qinghai Lake), aiming to elucidate the seasonal fossil and non-fossil sources and atmospheric processes of organic aerosols.

2. Methods

2.1. Sampling

Sampling was conducted at Qinghai Lake (37.04°N, 99.74°E, 3,200 m a.s.l.), a remote site in the northeastern TP. Although it is a remote site, there are two national highways (13–55 km away) as well as four counties (i.e., Gangcha, Haiyan, Gonhe, and Tianjun) around the Qinghai Lake, with a total population of ∼240,000. Local sources include residential burning activities and vehicles. Urban areas of Xining are located ∼180 km southeast of the Qinghai Lake. Total suspended particle (TSP) samples were collected weekly on pre-combusted quartz fiber filters (20.3 cm × 25.4 cm; QM-A, Whatman Inc.) using a high-volume aerosol sampler (TH150-A, Wuhan Tianhong INST Group) from September 2018 to August 2019. Blank filters were collected in each season exactly like the sample filters except that no air was drawn through the filter. The filters were individually wrapped in aluminum foils, packed in airtight polyethylene bags, and stored at −20°C for subsequent analysis. The real-time concentrations of PM_{10} and $PM_{2.5}$ were measured at Haiyan County and obtained from China National Environmental Monitoring Centre. Equivalent black carbon (eBC) concentrations were measured using an Aethalometer (Model AE33, Magee Scientific) (see Text S1 in Supporting Information S1).

2.2. Analytical Methods

OC and EC concentrations were measured using a thermo-optical carbon analyzer (Model 5, Sunset Laboratory Inc.) applying the EUSAAR_2 protocol (Cavalli et al., 2010), as detailed in Text S1 in Supporting Information S1.

For analysis of carbon isotope, a subset of 12 samples (3 samples per season) with varying loading of CAs were selected to represent different pollution conditions. The 12 samples cover 98 days, including 10 samples with weekly time resolution and 2 composite samples. Each composite sample combines two weekly samples collected during periods with similar TC (= OC + EC) concentrations (relative differences <15%) and similar back trajectories (Table S1 in Supporting Information S1). The analysis of stable carbon isotope composition ($\delta^{13}C$) was conducted by linking a carbon analyzer (Model 5, Sunset Laboratory Inc.) with a continuous flow isotope ratio mass spectrometer (IRMS; 652 Optima, Isoprime Ltd.; Dusek et al., 2013), including $\delta^{13}C$ of EC (Yao, Huang, et al., 2022; Yao, Ni, et al., 2022) as well as OC that desorbs in He at three consecutive temperature steps of 200°C, 350°C, and 550°C (Zenker et al., 2020).

For ^{14}C analysis, OC and EC were first converted to CO_2 using an aerosol combustion system (Dusek et al., 2019), followed by the ^{14}C measurements using the Mini Carbon Dating System accelerator mass spectrometer at

the University of Groningen (Dee et al., 2019). The ^{14}C data are reported as fraction modern ($F^{14}C$; Reimer et al., 2004). The detailed measurement procedures and quality controls of $\delta^{13}C$ and $F^{14}C$ measurements were present in Texts S2–S4 of Supporting Information S1.

2.3. Source Apportionment Method

$F^{14}C$ of OC and EC allows for the clear separation between the relative contributions of fossil (f_{fossil}(OC), f_{fossil}(EC)) and non-fossil sources (f_{nf}(OC), f_{bb}(EC)). f_{nf}(OC) and f_{bb}(EC) can be calculated by dividing the sample $F^{14}C$ values through the corresponding values of non-fossil sources ($F^{14}C_{nf}$). $F^{14}C_{nf}$ values are estimated as 1.10 ± 0.05 for EC and 1.09 ± 0.05 for OC, as detailed in Ni et al. (2019), using the long-time observation of atmospheric $F^{14}C$ of CO_2 and a tree growth model.

The f_{fossil}(EC) is further divided into the fractions of EC produced from liquid fossil fuel combustion ($f_{liq.fossil}$) and coal combustion (f_{coal}). The two groups have their distinct ^{13}C source signatures and EC preserves the ^{13}C signature of emission sources, which allows for isotope-based quantification by the Bayesian Markov chain Monte Carlo (MCMC) simulations (Andersson, 2011; Andersson et al., 2015, 2020):

$$\begin{pmatrix} F^{14}C_{(EC)} \\ \delta^{13}C_{EC} \\ 1 \end{pmatrix} = \begin{pmatrix} F^{14}C_{nf} & F^{14}C_{liq.fossil} & F^{14}C_{coal} \\ \delta^{13}C_{bb} & \delta^{13}C_{liq.fossil} & \delta^{13}C_{coal} \\ 1 & 1 & 1 \end{pmatrix} \begin{pmatrix} f_{bb} \\ f_{liq.fossil} \\ f_{coal} \end{pmatrix}. \quad (1)$$

$F^{14}C_{liq.fossil}$ and $F^{14}C_{coal}$ are 0, and $F^{14}C_{nf}$ is 1.10 ± 0.05, as explained above. The best estimate of ^{13}C source signatures of EC is established in Text S5 of Supporting Information S1 through a literature search: $\delta^{13}C_{liq.fossil}$ (-27.0 ± 1.0‰), $\delta^{13}C_{coal}$ (-23.8 ± 1.2‰), and $\delta^{13}C_{bb}$ (-27.1 ± 1.7‰ for C3 plants, -14.9 ± 1.7‰ for C4 plant). Uncertainties of both measurements ($F^{14}C_{(EC)}$ and $\delta^{13}C_{EC}$) and source signatures of EC are accounted for in the MCMC simulations. The MCMC was run for 10,000 iterations, with a burn-in of 1,000 and a data thinning of 10. With this setup, convergence diagnostics were established to make sure the good MCMC convergence. The MCMC results are the posterior probability density functions (PDFs) of f_{bb}, $f_{liq.fossil}$, and f_{coal}. The PDFs' median and interquartile range (25%–75%) represent the best estimate and variability, respectively. The ^{13}C source signatures are not as well constrained as ^{14}C. The potential influence of ^{13}C source signatures on the MCMC results was explored in a sensitivity analysis (Text S6 in Supporting Information S1). It shows that our best estimate scenario is relatively robust.

With ^{14}C-determined f_{bb}(EC) and f_{nf}(OC), EC and OC were resolved into fossil and non-fossil EC and OC (EC_{fossil}, EC_{bb}, OC_{fossil}, and OC_{nf}). With the MCMC-derived $f_{liq.fossil}$ and f_{coal}, EC_{fossil} can further be separated into $EC_{liq.fossil}$ and EC_{coal}. OC_{fossil} and OC_{nf} were further apportioned into OC_{fossil} from primary and secondary sources (POC_{fossil} and SOC_{fossil}, respectively), OC_{nf} from primary biomass-burning (POC_{bb}) and other non-fossil sources ($OC_{o,nf}$). $OC_{o,nf}$ includes secondary OC_{nf} (SOC_{nf}), primary biogenic OC, and cooking OC. Due to the sparse population in the TP, cooking OC is expected to be of minor importance. Based on analysis of tracers of primary biogenic aerosol particles (including arabitol, mannitol, and glucose), the concentrations of the fungal-spore-derived OC and plant-debris OC were estimated as 74 ± 49 ng m^{-3}, accounting for only $1.7\% \pm 2.1\%$ OC during our sampling campaign. This suggests low abundance of primary biogenic OC. Therefore, $OC_{o,nf}$ is an approximation of SOC_{nf} or a upper limit of SOC_{nf}. Total SOC was thus estimated as the sum of SOC_{fossil} and $OC_{o,nf}$. The equations for detailed source apportionment are shown in Table S2 of Supporting Information S1.

3. Result and Discussion

3.1. Seasonal Variability

The particulate air pollution at Qinghai Lake showed large seasonal variability. The yearly minima in concentrations of PM_{10}, $PM_{2.5}$, and equivalent BC (eBC, i.e., an optically based analog of mass-based EC) were typically observed during the monsoon season (Figure S1 in Supporting Information S1). Not only increased wet scavenging (Figure S2 in Supporting Information S1), but also decreased human activities for heating (e.g., biomass burning, coal combustion) lead to reduced emissions in the monsoon season. These findings are in qualitative agreement with previous investigations at Qinghai Lake, as well as other sites in the TP (Cong et al., 2015; Xiang

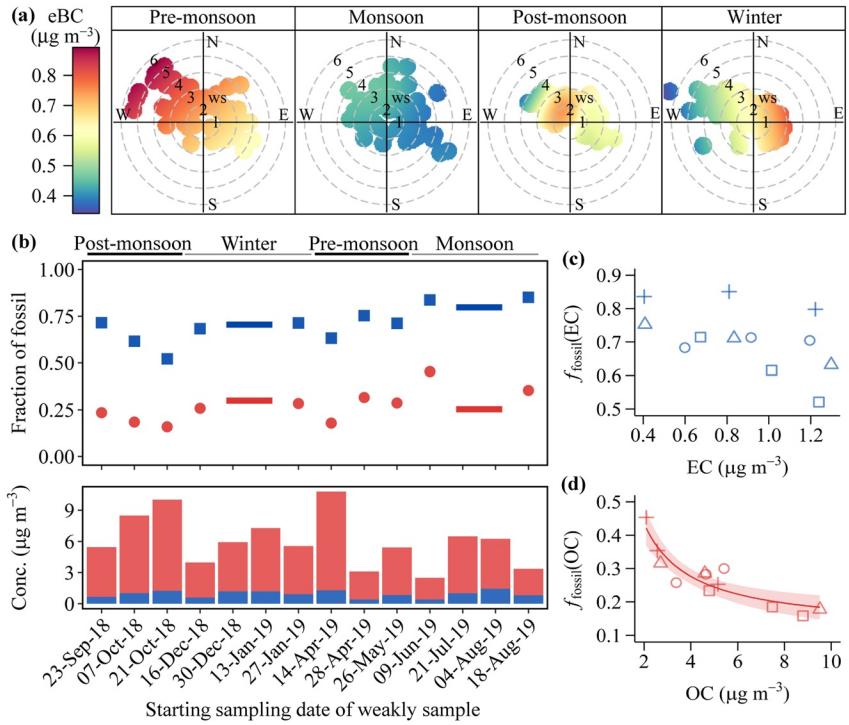

Figure 1. (a) Bivariate polar plot that illustrates the seasonal variation of mass concentrations of equivalent BC (eBC) as a function of wind speed (m s^{-1}) and wind direction, (b) fraction of fossil carbon in elemental carbon (EC) and organic carbon (OC; f_{fossil}(EC) and f_{fossil}(OC), respectively) as well as mass concentrations of EC and OC for each weekly sample, (c) scatter plot of f_{fossil}(EC) against EC concentrations, (d) scatter plot of f_{fossil}(OC) against OC concentrations in different seasons during 2018–2019 at Qinghai Lake.

et al., 2021; Zhao et al., 2013). The considerable seasonal variation in particle concentrations occurs because of varying emission sources and differences in aerosol lifetimes in different seasons. In the pre-monsoon season, the high eBC was associated with strong wind from west and northwest sectors in the bivariate polar plot (Figure 1a), suggesting probable impacts from regional transport. In the rainy monsoon season, the BC lifetime is expected to be shorter, which would mean a weak influence from regional transport and a more pronounced influence from local sources. In post-monsoon and winter, elevated eBC concentrations mainly occur at low wind speed (<3 m s^{-1}), indicating the important contribution of local/regional emissions. It has been shown that in addition to regional transport, local sources are also an important contributor to CAs in the TP (Li et al., 2016; Li, Zhang, et al., 2022). This study observed the annual mean eBC of 0.60 ± 0.28 μg m^{-3} during 2018/2019 at Qinghai Lake, northeastern TP, similar to the concurrent observation in Beiluhe, central TP (0.61 ± 0.32 μg m^{-3}). eBC concentrations were higher during 2019/2020 in Ngari, southwestern TP (1.08 ± 0.76 μg m^{-3}), where polluted air masses from northern India played a role (Zhu et al., 2021).

3.2. ^{14}C-Based Source Apportionment of OC and EC

Radiocarbon allows for quantifying the relative contribution of fossil and non-fossil sources with high precision, regardless of atmospheric processing. For the 1-yr study period, the concentration-weighted ^{14}C-based relative contribution of fossil sources to EC (f_{fossil}(EC)) was 70% ± 10% (± weighted SD) with a large seasonal variability (Figure 1b). We find high fossil contributions to EC during the monsoon season (82% ± 3%), with the remaining EC contributed by biomass burning, showing a strong impact from fossil fuel combustion in the monsoon season. This is mainly due to higher contribution of liquid fossil fuel sources to EC in the monsoon season as discussed in Section 3.3. In the pre-monsoon and post-monsoon season, the fossil contributions to EC were lower (68% ± 6% and 60% ± 9%, respectively), and decreased with the increase in EC concentrations (Figure 1c). The f_{fossil}(EC) in winter was relatively stable (70% ± 1%) and did not vary with EC concentrations. The seasonal variation of f_{fossil}(EC) was driven by a clear seasonal cycle of biomass-burning EC at Qinghai

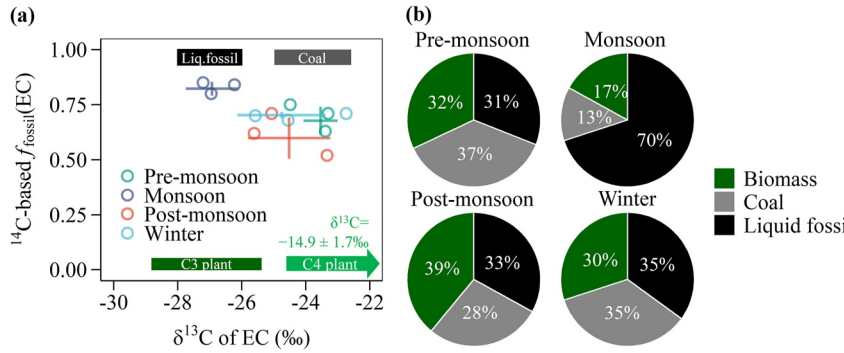

Figure 2. (a) ^{14}C-based fraction of fossil carbon in elemental carbon (EC; f_{fossil}(EC)) versus δ^{13}C of EC (‰) in different seasons. Centers of cross bars indicate the weighted mean of measured samples in each season, and the length of bars represent one weighed standard deviation. The expected ^{14}C and ^{13}C source signatures (i.e., endmembers) of EC from liquid fossil fuel combustion, coal combustion, and C3 plant burning (Text S5 in Supporting Information S1) are shown as black, gray, and green bars, respectively. The ^{13}C signature of C4 plant burning ($\delta^{13}C = -14.9 \pm 1.7‰$) is also indicated. (b) Source apportionment results of EC, derived by the δ^{13}C- and F^{14}C -based Bayesian Markov chain Monte Carlo simulations (Section 2.3).

Lake. The seasonal mean biomass-burning EC concentrations (EC_{bb}) varied by three times from 0.14 μg m^{-3} in the monsoon season to 0.39 μg m^{-3} in the post-monsoon season, larger than the variation of fossil-derived EC (EC_{fossil} = 0.57–0.67 μg m^{-3}).

The fossil contributions to OC (f_{fossil}(OC)) increased with increasing f_{fossil}(EC), but were consistently smaller than those to EC (Figure S3 in Supporting Information S1). f_{fossil}(OC) showed a similar seasonal pattern with f_{fossil}(EC), with higher f_{fossil}(OC) in the monsoon season (32% ± 10%) and lower in the post-monsoon season (19% ± 4%). Despite the seasonality, f_{fossil}(OC) highly correlates with the inverse of OC concentrations ($R^2 = 0.83$, $p < 0.001$; Figure 1d), suggesting that the atmospheric OC concentrations reflect the combined contribution of the OC background and the additional non-background OC source that contributed to increases in atmospheric OC at Qinghai Lake (Keeling, 1958, 1961). This inverse relation gives a f_{fossil}(OC) of 12% as OC concentrations approach infinity, showing that the non-background OC source was mainly of non-fossil origin. In winter, although the f_{fossil}(OC) and OC concentrations agreed with the overall inverse trend, they showed the opposite trend that f_{fossil}(OC) increased with the increase in OC concentration, signifying an important contribution of fossil sources to the OC increment in winter. The f_{fossil}(OC) and f_{fossil}(EC) reported here are generally larger than those in other remote areas of southern TP (e.g., Nam Co and Zhongba) that more influenced by biomass burning within the TP and from South Asia, but smaller than those in Lhasa, a typical polluted city in the southern TP (Figure S4 in Supporting Information S1; Li et al., 2016; Li, Bosch, et al., 2022). Despite being higher than at other remote sites of the TP, our f_{fossil}(EC) was only a little lower than that of East China (e.g., ∼80% in Beijing; Andersson et al., 2015; B. Chen et al., 2013; Zhang et al., 2015), probably associated with contributions of regional transport from east as indicated in the bivariate polar plot (Figure 1a).

3.3. Stable Carbon Isotope Composition of EC

The ^{13}C signature of EC does not change in the atmosphere, and it is thus the result of source mixing. In our samples, all the δ^{13}C of EC overlapped with the endmembers of C3 plant burning, liquid fossil fuel combustion (e.g., traffic) and coal combustion (Figure 2a). C4 plant burning also contributed to EC in Qinghai Lake, evidenced by some enriched $\delta^{13}C_{EC}$ datapoints (e.g., the maximum $\delta^{13}C_{EC}$ of −22.7‰ in winter) that were on the higher end of coal combustion endmember ($\delta^{13}C_{coal}$ = −23.8 ± 1.2‰). The $\delta^{13}C_{EC}$ showed considerable seasonal changes: it was most depleted in ^{13}C in the monsoon season (−26.9 ± 0.8‰), and higher in winter (−24.8 ± 1.4‰) and the post-monsoon season (−24.5 ± 1.3‰), with the most enriched values in the pre-monsoon season (−23.5 ± 0.5‰). With the depleted ^{13}C signatures of EC, the higher fossil contribution to EC in the monsoon season was further attributed to the significant influence of liquid fossil fuel combustion ($\delta^{13}C_{liq.fossil}$ = −27.0 ± 1.0‰). $\delta^{13}C_{EC}$ in other seasons was comparable to the ^{13}C source signature of coal combustion, pointing to a larger influence of coal combustion. Compared with the only other seasonal observations on $\delta^{13}C_{EC}$ in the TP, a much smaller seasonal variation of $\delta^{13}C_{EC}$ within 1‰ was found in Lhasa, a typical polluted city (Figure S4 in Supporting Information S1; Li et al., 2016).

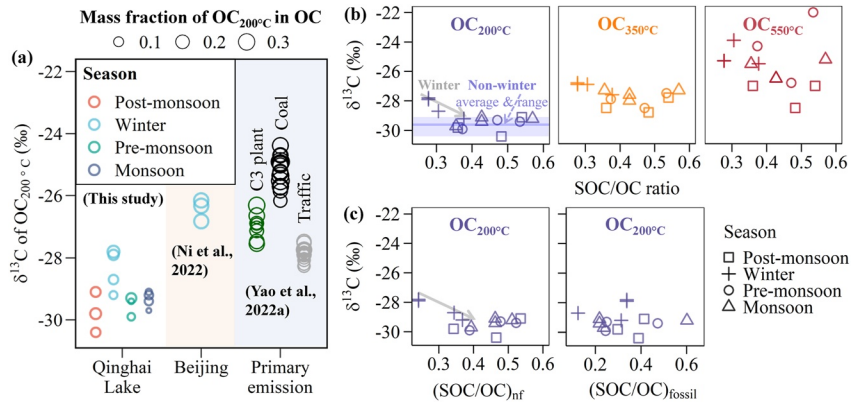

Figure 3. (a) $\delta^{13}C$ of organic carbon (OC) desorbed at 200°C ($OC_{200°C}$) in Qinghai Lake (this study) and Beijing (Ni et al., 2022), as well as in the primary emission of C3 plant burning, coal combustion and traffic in China (Yao, Huang, et al., 2022). The symbol size in panel (a) is proportional to the mass fraction of $OC_{200°C}$ in total OC (i.e., OC determined by the EUSAAR_2 protocol). Panels (b and c) show the scatter plots of SOC/OC ratios versus $\delta^{13}C$ of $OC_{200°C}$, $OC_{350°C}$, and $OC_{550°C}$ in different seasons. For secondary OC (SOC) estimation, see details in Section 2.3. $(SOC/OC)_{nf}$, non-fossil SOC/OC ratio; $(SOC/OC)_{fossil}$, fossil SOC/OC ratio.

The Bayesian MCMC results show that liquid fossil fuel combustion accounted for ~70% of EC in the monsoon season, and the contribution is reduced by half in other seasons (Figure 2b). We also found that coal combustion and biomass burning contributed roughly equally to EC in the monsoon season (13% and 17%, respectively); their contributions increased by around two to three times in other seasons. Despite the fairly constant EC_{fossil} (i.e., the sum of EC_{coal} and $EC_{liq.fossil}$) concentrations in different seasons, EC_{coal} and $EC_{liq.fossil}$ showed large seasonal variations, with minimum EC_{coal} and maximum $EC_{liq.fossil}$ in the monsoon season (Figure S5 in Supporting Information S1). The high $EC_{liq.fossil}$ concentration in the monsoon season was consistent with increased number of tourist vehicles in the tourism rush season at Qinghai Lake (L. Hu et al., 2021).

3.4. Stable Carbon Isotope Composition of OC as a Function of Thermal Refractiveness

Unlike EC, the ^{13}C signature of OC reflects the integrated effects of source mixing as well as atmospheric processing (e.g., secondary formation and photochemical oxidation) via the kinetic isotope effect. OC desorbed at three different temperature steps of 200°C, 350°C, and 550°C (i.e., $OC_{200°C}$, $OC_{350°C}$, and $OC_{550°C}$), approximately separating OC according to volatility (Ma et al., 2016), had different $\delta^{13}C$ values ranging from $-29.2 \pm 0.9‰$ for $\delta^{13}C_{OC,200}$ to $-27.9 \pm 0.7‰$ for $\delta^{13}C_{OC,350}$ to $-26.2 \pm 1.5‰$ for $\delta^{13}C_{OC,550}$. In contrast, source samples from a single source usually do not show such large differences between $\delta^{13}C_{OC}$ values at different temperature steps (<2‰; Yao, Huang, et al., 2022; Zenker et al., 2020). At Qinghai Lake, this large difference in $\delta^{13}C_{OC}$ values at different desorption temperatures indicates the varying contribution of sources and atmospheric processes to the different OC volatility fractions.

Overall, $OC_{550°C}$ and $OC_{350°C}$ were comparable large mass fraction of OC, constituting 25% and 26% of total OC, respectively. $OC_{200°C}$ was the smallest fraction for all seasons (~6% of total OC). $OC_{200°C}$, $OC_{350°C}$, and $OC_{550°C}$ do not add up to total OC, because a portion of OC forms charred OC that cannot be desorbed in helium. The larger mass fraction of $OC_{200°C}$, the more volatile OC is, because more volatile compounds tend to desorb at lower temperatures. Usually, freshly emitted POC and newly formed SOC are more volatile than aged OC that has been modified in the atmosphere by extensive photochemical processing (Keller & Burtscher, 2017; Masalaite et al., 2020; Meusinger et al., 2017). The mass fraction of $OC_{200°C}$ in total OC at Qinghai Lake was smaller than that in urban Beijing and much smaller than for primary emissions (Figure 3a), probably due to active photochemical processing of OC emissions under strong solar radiation over the TP (Yang et al., 2014). On the other hand, the mass fraction of $OC_{200°C}$ was higher (i.e., OC was more volatile) in the post-monsoon season and winter than in the pre-monsoon and monsoon season. This could be caused by lower temperature in winter (Figure S2 in Supporting Information S1) that promotes partitioning of semi-volatile OC to the condensed phase. In addition, increased solar radiation in the pre-monsoon and monsoon season (Table S1 in Supporting Information S1) led to enhanced photochemical activity and thus less volatile OC (Masalaite et al., 2020). This is also consistent with

our laboratory studies, where source samples were aged in a small reactor under UV light, that photolysis causes mainly mass loss in $OC_{200°C}$ relative to OC that desorbs at higher temperatures (Ettinger, 2022).

Recently formed SOC is considered to be ^{13}C-depleted, whereas aged OC is enriched in ^{13}C (Dasari et al., 2019; Fisseha et al., 2009; Irei et al., 2006; Kirillova et al., 2013; Pavuluri & Kawamura, 2016). In our samples, the most strongly depleted $\delta^{13}C_{OC,200}$ values fall out of the ranges of ^{13}C signatures of anthropogenic primary emission (Figure 3a). The most likely explanation for the strongly depleted $\delta^{13}C_{OC,200}$ is the formation of (biogenic) SOC that has depleted (more negative) ^{13}C signature and contributes strongly to the more volatile fraction. More depleted $\delta^{13}C$ values of OC at lower desorption temperature was also found for urban aerosols in Beijing, China (Ni et al., 2022) and Naples, Italy (Zenker et al., 2020), as well as urban, coastal, and forest aerosols in Lithuania (Masalaite et al., 2017, 2020).

Our $\delta^{13}C_{OC,200}$ values varied with seasons, with the less depleted values in winter compared with other seasons (Figure 3). In winter, OC contained less SOC than that in other seasons (Figure 3b), and the $\delta^{13}C$ of $OC_{200°C}$ showed a tendency toward depleted values with increased SOC/OC ratios. The largest SOC/OC ratios was 0.38 in winter, characterized by the most depleted $\delta^{13}C_{OC,200}$ of −29.2‰. The SOC/OC ratios were further increased in other seasons (i.e., non-winter seasons) up to 0.57; however, $\delta^{13}C_{OC,200}$ values did not further decrease, and converged to a narrow range of −30.4‰ to −29.1‰. A similar trend was also observed for $\delta^{13}C_{OC,200}$ versus non-fossil SOC/OC ratio, but not present for $\delta^{13}C_{OC,200}$ versus fossil SOC/OC ratio. This again indicates the importance of non-fossil secondary sources on the variation of $\delta^{13}C_{OC,200}$.

Much more depleted than $\delta^{13}C_{OC,200}$ for anthropogenic primary emissions, our $\delta^{13}C_{OC,200}$ in non-winter seasons (weighted average: −29.6‰; range: −30.4‰ to −29.1‰) is a potential ^{13}C signature for SOC under strong solar radiation in a remote area. The relatively depleted $\delta^{13}C_{OC,200}$ values in non-winter seasons are in line with the $\delta^{13}C$ of $OC_{200°C}$ during the clean period in summer at a forest site in Lithuania (−29.6 ± 0.5‰; Masalaite et al., 2020) and total SOC from β-pinene oxidation (−29.6‰; Fisseha et al., 2009), and are a slightly heavier than the $\delta^{13}C$ values of SOC from toluene (−31.6‰ to −32.3‰; Irei et al., 2006).

In winter, the $OC_{200°C}$ fraction at Qinghai Lake was lower and ∼1.7‰ depleted in ^{13}C compared to $OC_{200°C}$ in urban Beijing (Figure 3a). This is probably due to the proximity of primary emission sources in the urban environment, which have higher $\delta^{13}C$ values than SOC and lead to higher $OC_{200°C}$ amounts due to less aging times. $\delta^{13}C_{OC,350}$ values varied in a small range within 2‰ for all samples in all seasons, and did not change significantly with SOC/OC ratios (Figure 3b and Figure S6 in Supporting Information S1). In contrast, $\delta^{13}C$ of $OC_{550°C}$, the less volatile OC fraction, varied in a wide range from −28.5‰ to −22‰, but did not show any correlation with SOC/OC ratios. $\delta^{13}C_{OC,550}$ was more enriched in ^{13}C (up to −22‰) compared with $\delta^{13}C_{OC,350}$ and $\delta^{13}C_{OC,200}$, suggesting the contribution of specific sources with high $\delta^{13}C$ values to $OC_{550°C}$. However, our ^{13}C signature of EC shows that coal combustion (−21‰ to −25‰; Widory, 2006), a relatively ^{13}C-enriched source, was not a dominant source. The enriched $\delta^{13}C_{OC,550}$ was therefore related to the atmospheric aging processes that leading to ^{13}C enrichment (Dasari et al., 2019; Irei et al., 2011; Pavuluri & Kawamura, 2016). This finding is consistent with previous observations in ambient atmosphere and our laboratory studies (Ettinger, 2022; Masalaite et al., 2020; Ni et al., 2022).

4. Conclusions and Implications

Observational constraints on sources and formation of CAs are scarce and rarely extend over more than one season in the TP. This study presents the first year-round dual-carbon isotopic analysis of CAs in the northeastern TP (Qinghai Lake). EC was dominated by fossil sources (70% ± 10%), while non-fossil sources contributed more strongly to OC (76% ± 7%). ^{14}C results also show that there was a relatively stable background aerosol with a relatively strong contribution of fossil sources and a non-background source of non-fossil origins. This drives a large seasonality in both concentrations and sources of EC and OC, with lower concentrations and higher fossil contribution in the monsoon season. An opposite seasonality of EC sources was previously found in the Arctic, though with comparable fossil contribution (69% ± 19%; Winiger et al., 2017). Fossil contributions to EC and OC were lower in the southern TP that are more influenced by biomass burning within the TP and from South Asia (Li et al., 2016; Li, Bosch, et al., 2022), highlighting the spatially heterogeneous of local sources and transport over the TP. Therefore, high-resolution emission inventories specifically for TP are needed to better characterize locally sourced CAs.

The observed OC at Qinghai Lake was less volatile than OC found in primary emissions and in urban areas, reflecting highly processed OC under strong solar radiation. Large differences were found in ^{13}C of different OC volatility fractions. More volatile OC was depleted in ^{13}C by as much as 3‰ relative to less volatile OC. This difference is caused by the kinetic isotopic effect in atmospheric processes. First, SOA compounds, which are depleted in ^{13}C, contributed strongly to more volatile OC (-29.2 ± 0.9‰). This influence of secondary formation was further justified by the negative correlation between $\delta^{13}C$ and SOC/OC ratios, providing observational evidence for ^{13}C-depleted SOC besides few laboratory studies, for example, $\delta^{13}C$ of SOC from β-pinene oxidation (−29.6‰; Fisseha et al., 2009) and toluene (−31.6‰ to −32.3‰; Irei et al., 2006). On the other hand, photochemical aging played an important role in the less volatile OC, evidenced by the enriched $\delta^{13}C$ values (up to −22‰) that cannot be explained by primary source mixing. This is consistent with what we expect from photolysis with strong UV light (Ettinger, 2022). The ^{13}C signature of OC thus provides a strong basis to investigate aerosol processing. However, isotopic fractionation induced by atmospheric processes is not quantitatively constrained and needs further laboratory investigations.

TSP samples are used in this study, however, sources and transformations of CAs in $PM_{2.5}$ are probably different due to different particle sizes (Li, Zhang, et al., 2022). Therefore, in the future, $PM_{2.5}$ needs to be investigated to more comprehensively understand CAs over TP. Together, this study provides observational constraints on sources and atmospheric processes of CAs in a climatically sensitive region, thereby facilitating improved modeling of aerosol climate effects.

Data Availability Statement

Data used in this study can be accessed online (at https://doi.org/10.5281/zenodo.7380212).

Acknowledgments
The authors acknowledge the project grants from the National Natural Science Foundation of China (Grants 41771518, 41925015, 91644219, and 41877408), the KNAW (Grant 530-5CDP30), the Chinese Academy of Sciences (Grant ZDBS-LY-DQC001), and the Cross Innovative Team fund from the State Key Laboratory of Loess and Quaternary Geology (Grant SKLLQGTD1801). We thank Dipayan Paul and Marc Bleeker for their help with the ^{14}C measurements. Special thanks are given to Henk Jansen, Dipayan Paul, and Marc Bleeker for their help with the TOA-IRMS modification and tests at CIO, and to Romke Tjoelker and Katrin Zenker for developing the connection interface of TOA-IRMS at CIO.

References

Aggarwal, S. G., & Kawamura, K. (2009). Carbonaceous and inorganic composition in long-range transported aerosols over northern Japan: Implication for aging of water-soluble organic fraction. *Atmospheric Environment*, *43*(16), 2532–2540. https://doi.org/10.1016/j.atmosenv.2009.02.032

Andersson, A. (2011). A systematic examination of a random sampling strategy for source apportionment calculations. *Science of the Total Environment*, *412*, 232–238. https://doi.org/10.1016/j.scitotenv.2011.10.031

Andersson, A., Deng, J., Du, K., Zheng, M., Yan, C., Sköld, M., & Gustafsson, O. (2015). Regionally-varying combustion sources of the January 2013 severe haze events over eastern China. *Environmental Science & Technology*, *49*(4), 2038–2043. https://doi.org/10.1021/es503855e

Andersson, A., Kirillova, E. N., Decesari, S., DeWitt, L., Gasore, J., Potter, K. E., et al. (2020). Seasonal source variability of carbonaceous aerosols at the Rwanda Climate Observatory. *Atmospheric Chemistry and Physics*, *20*(8), 4561–4573. https://doi.org/10.5194/acp-20-4561-2020

Bond, T., Doherty, S., Fahey, D., Forster, P., Berntsen, T., DeAngelo, B., et al. (2013). Bounding the role of black carbon in the climate system: A scientific assessment. *Journal of Geophysical Research: Atmospheres*, *118*(11), 5380–5552. https://doi.org/10.1002/jgrd.50171

Cavalli, F., Viana, M., Yttri, K. E., Genberg, J., & Putaud, J.-P. (2010). Toward a standardized thermal-optical protocol for measuring atmospheric organic and elemental carbon: The EUSAAR protocol. *Atmospheric Measurement Techniques*, *3*(1), 79–89. https://doi.org/10.5194/amt-3-79-2010

Chen, B., Andersson, A., Lee, M., Kirillova, E. N., Xiao, Q., Kruså, M., et al. (2013). Source forensics of black carbon aerosols from China. *Environmental Science & Technology*, *47*(16), 9102–9108. https://doi.org/10.1021/es401599r

Cong, Z., Kang, S., Kawamura, K., Liu, B., Wan, X., Wang, Z., et al. (2015). Carbonaceous aerosols on the south edge of the Tibetan Plateau: Concentrations, seasonality and sources. *Atmospheric Chemistry and Physics*, *15*(3), 1573–1584. https://doi.org/10.5194/acp-15-1573-2015

Dasari, S., Andersson, A., Bikkina, S., Holmstrand, H., Budhavant, K., Satheesh, S., et al. (2019). Photochemical degradation affects the light absorption of water-soluble brown carbon in the South Asian outflow. *Science Advances*, *5*(1), eaau8066. https://doi.org/10.1126/sciadv.aau8066

Dee, M., Palstra, S., Aerts-Bijma, A., Bleeker, M., De Bruijn, S., Ghebru, F., et al. (2019). Radiocarbon dating at Groningen: New and updated chemical pretreatment procedures. *Radiocarbon*, *62*(1), 63–74. https://doi.org/10.1017/RDC.2019.101

Dusek, U., Cosijn, M. M., Ni, H., Huang, R.-J., Meijer, H. A. J., & van Heuven, S. (2019). Technical Note: An automated system for separate combustion of elemental and organic carbon for ^{14}C analysis of carbonaceous aerosol. *Aerosol and Air Quality Research*, *19*(11), 2604–2611. https://doi.org/10.4209/aaqr.2019.06.0287

Dusek, U., Meusinger, C., Oyama, B., Ramon, W., de Wilde, P., Holzinger, R., & Röckmann, T. (2013). A thermal desorption system for measuring $\delta^{13}C$ ratios on organic aerosol. *Journal of Aerosol Science*, *66*, 72–82. https://doi.org/10.1016/j.jaerosci.2013.08.005

Ettinger, N. v. (2022). *Evaluating the potential of the ^{13}C-signature of organic aerosols to determine the effect of photochemical aging reactions, (Master's thesis)*. University of Groningen. Retrieved from https://fse.studenttheses.ub.rug.nl/id/eprint/26668

Fisseha, R., Spahn, H., Wegener, R., Hohaus, T., Brasse, G., Wissel, H., et al. (2009). Stable carbon isotope composition of secondary organic aerosol from β-pinene oxidation. *Journal of Geophysical Research: Atmospheres*, *114*(D2), D02304. https://doi.org/10.1029/2008JD011326

Fuzzi, S., Andreae, M. O., Huebert, B. J., Kulmala, M., Bond, T. C., Boy, M., et al. (2006). Critical assessment of the current state of scientific knowledge, terminology, and research needs concerning the role of organic aerosols in the atmosphere, climate, and global change. *Atmospheric Chemistry and Physics*, *6*(7), 2017–2038. https://doi.org/10.5194/acp-6-2017-2006

Gustafsson, Ö., & Ramanathan, V. (2016). Convergence on climate warming by black carbon aerosols. *Proceedings of the National Academy of Sciences*, *113*(16), 4243–4245. https://doi.org/10.1073/pnas.1603570113

Hu, L., Xu, J., Bao, C., & Pei, T. (2021). Influential factor detection for tourism on the Qinghai-Tibet Plateau based on social media data. *ISPRS International Journal of Geo-Information*, *10*(9), 579. https://doi.org/10.3390/ijgi10090579

Irei, S., Huang, L., Collin, F., Zhang, W., Hastie, D., & Rudolph, J. (2006). Flow reactor studies of the stable carbon isotope composition of secondary particulate organic matter generated by OH-radical-induced reactions of toluene. *Atmospheric Environment*, *40*(30), 5858–5867. https://doi.org/10.1016/j.atmosenv.2006.05.001

Irei, S., Rudolph, J., Huang, L., Auld, J., & Hastie, D. (2011). Stable carbon isotope ratio of secondary particulate organic matter formed by photooxidation of toluene in indoor smog chamber. *Atmospheric Environment*, *45*(4), 856–862. https://doi.org/10.1016/j.atmosenv.2010.11.021

Kanakidou, M., Seinfeld, J. H., Pandis, S. N., Barnes, I., Dentener, F. J., Facchini, M. C., et al. (2005). Organic aerosol and global climate modeling: A review. *Atmospheric Chemistry and Physics*, *5*(4), 1053–1123. https://doi.org/10.5194/acp-5-1053-2005

Keeling, C. D. (1958). The concentration and isotopic abundances of atmospheric carbon dioxide in rural areas. *Geochimica et Cosmochimica Acta*, *13*(4), 322–334. https://doi.org/10.1016/0016-7037(58)90033-4

Keeling, C. D. (1961). The concentration and isotopic abundances of carbon dioxide in rural and marine air. *Geochimica et Cosmochimica Acta*, *24*(3), 277–298. https://doi.org/10.1016/0016-7037(61)90023-0

Keller, A., & Burtscher, H. (2017). Characterizing particulate emissions from wood burning appliances including secondary organic aerosol formation potential. *Journal of Aerosol Science*, *114*, 21–30. https://doi.org/10.1016/j.jaerosci.2017.08.014

Kirillova, E. N., Andersson, A., Sheesley, R. J., Kruså, M., Praveen, P. S., Budhavant, K., et al. (2013). ^{13}C- and ^{14}C-based study of sources and atmospheric processing of water-soluble organic carbon (WSOC) in South Asian aerosols. *Journal of Geophysical Research: Atmospheres*, *118*(2), 614–626. https://doi.org/10.1002/jgrd.50130

Kuang, X., & Jiao, J. J. (2016). Review on climate change on the Tibetan Plateau during the last half century. *Journal of Geophysical Research: Atmospheres*, *121*(8), 3979–4007. https://doi.org/10.1002/2015JD024728

Li, C., Bosch, C., Kang, S., Andersson, A., Chen, P., Zhang, Q., et al. (2016). Sources of black carbon to the Himalayan–Tibetan Plateau glaciers. *Nature Communications*, *7*(1), 12574. https://doi.org/10.1038/ncomms12574

Li, C., Bosch, C., Kang, S., Andersson, A., Chen, P., Zhang, Q., et al. (2022). ^{14}C characteristics of organic carbon in the atmosphere and at glacier region of the Tibetan Plateau. *Science of the Total Environment*, *832*, 155020. https://doi.org/10.1016/j.scitotenv.2022.155020

Li, C., Chen, P., Kang, S., Yan, F., Tripathee, L., Wu, G., et al. (2018). Fossil fuel combustion emission from South Asia influences precipitation dissolved organic carbon reaching the remote Tibetan Plateau: Isotopic and molecular evidence. *Journal of Geophysical Research: Atmospheres*, *123*(11), 6248–6258. https://doi.org/10.1029/2017JD028181

Li, C., Zhang, C., Yan, F., Kang, S., Xu, Y., Liu, Y., et al. (2022). Importance of local non-fossil sources to carbonaceous aerosols at the eastern fringe of the Tibetan Plateau, China: Δ^{14}C and δ^{13}C evidences. *Environmental Pollution*, *311*, 119858. https://doi.org/10.1016/j.envpol.2022.119858

Ma, J., Li, X., Gu, P., Dallmann, T. R., Presto, A. A., & Donahue, N. M. (2016). Estimating ambient particulate organic carbon concentrations and partitioning using thermal optical measurements and the volatility basis set. *Aerosol Science and Technology*, *50*(6), 638–651. https://doi.org/10.1080/02786826.2016.1158778

Masalaite, A., Holzinger, R., Remeikis, V., Roeckmann, T., & Dusek, U. (2017). Characteristics, sources and evolution of fine aerosol (PM_1) at urban, coastal and forest background sites in Lithuania. *Atmospheric Environment*, *148*, 62–76. https://doi.org/10.1016/j.atmosenv.2016.10.038

Masalaite, A., Remeikis, V., Zenker, K., Westra, I., Meijer, H. A. J., & Dusek, U. (2020). Seasonal changes of sources and volatility of carbonaceous aerosol at urban, coastal and forest sites in Eastern Europe (Lithuania). *Atmospheric Environment*, *225*, 117374. https://doi.org/10.1016/j.atmosenv.2020.117374

Meusinger, C., Dusek, U., King, S. M., Holzinger, R., Rosenørn, T., Sperlich, P., et al. (2017). Chemical and isotopic composition of secondary organic aerosol generated by α-pinene ozonolysis. *Atmospheric Chemistry and Physics*, *17*(10), 6373–6391. https://doi.org/10.5194/acp-17-6373-2017

Ni, H., Huang, R.-J., Cao, J., Guo, J., Deng, H., & Dusek, U. (2019). Sources and formation of carbonaceous aerosols in Xi'an, China: Primary emissions and secondary formation constrained by radiocarbon. *Atmospheric Chemistry and Physics*, *19*(24), 15609–15628. https://doi.org/10.5194/acp-19-15609-2019

Ni, H., Huang, R.-J., Yao, P., Cosijn, M. M., Kairys, N., Zhong, H., & Dusek, U. (2022). Organic aerosol formation and aging processes in Beijing constrained by size-resolved measurements of radiocarbon and stable isotopic ^{13}C. *Environment International*, *158*, 106890. https://doi.org/10.1016/j.envint.2021.106890

Pavuluri, C. M., & Kawamura, K. (2016). Enrichment of ^{13}C in diacids and related compounds during photochemical processing of aqueous aerosols: New proxy for organic aerosols aging. *Scientific Reports*, *6*(1), 36467. https://doi.org/10.1038/srep36467

Reimer, P. J., Brown, T. A., & Reimer, R. W. (2004). Discussion: Reporting and calibration of post-bomb ^{14}C data. *Radiocarbon*, *46*(3), 1299–1304. https://doi.org/10.1017/S0033822200033154

Wang, G., Xie, M., Hu, S., Gao, S., Tachibana, E., & Kawamura, K. (2010). Dicarboxylic acids, metals and isotopic compositions of C and N in atmospheric aerosols from inland China: Implications for dust and coal burning emission and secondary aerosol formation. *Atmospheric Chemistry and Physics*, *10*(13), 6087–6096. https://doi.org/10.5194/acp-10-6087-2010

Widory, D. (2006). Combustibles, fuels and their combustion products: A view through carbon isotopes. *Combustion Theory and Modeling*, *10*(5), 831–841. https://doi.org/10.1080/13647830600720264

Winiger, P., Andersson, A., Eckhardt, S., Stohl, A., Semiletov, I. P., Dudarev, O. V., et al. (2017). Siberian Arctic black carbon sources constrained by model and observation. *Proceedings of the National Academy of Sciences*, *114*(7), E1054–E1061. https://doi.org/10.1073/pnas.1613401114

Winiger, P., Barrett, T. E., Sheesley, R. J., Huang, L., Sharma, S., Barrie, L. A., et al. (2019). Source apportionment of circum-Arctic atmospheric black carbon from isotopes and modeling. *Science Advances*, *5*(2). eaau8052. https://doi.org/10.1126/sciadv.aau8052

Xiang, Y., Zhang, T., Liu, J., Wan, X., Loewen, M., Chen, X., et al. (2021). Vertical profile of aerosols in the Himalayas revealed by lidar: New insights into their seasonal/diurnal patterns, sources, and transport. *Environmental Pollution*, *285*, 117686. https://doi.org/10.1016/j.envpol.2021.117686

Xu, B., Zhang, G., Gustafsson, Ö., Kawamura, K., Lin, J., Andersson, A., et al. (2021). Large contribution of fossil-derived components to aqueous secondary organic aerosols in China. *Nature Communication*, *13*(1), 5115. https://doi.org/10.1038/s41467-022-32863-3

Yang, K., Wu, H., Qin, J., Lin, C., Tang, W., & Chen, Y. (2014). Recent climate changes over the Tibetan Plateau and their impacts on energy and water cycle: A review. *Global and Planetary Change*, *112*, 79–91. https://doi.org/10.1016/j.gloplacha.2013.12.001

Yao, P., Huang, R.-J., Ni, H., Kairys, N., Yang, L., Meijer, H. A. J., & Dusek, U. (2022). ^{13}C signatures of aerosol organic and elemental carbon from major combustion sources in China compared to worldwide estimates. *Science of the Total Environment*, *810*, 151284. https://doi.org/10.1016/j.scitotenv.2021.151284

Yao, P., Ni, H., Paul, D., Masalaite, A., Huang, R.-J., Meijer, H. A. J., & Dusek, U. (2022). An automated method for thermal-optical separation of aerosol organic/elemental carbon for ^{13}C analysis at the sub-μgC level: A comprehensive assessment. *Science of the Total Environment*, *804*, 150031. https://doi.org/10.1016/j.scitotenv.2021.150031

Zenker, K., Sirignano, C., Riccio, A., Chianese, E., Calfapietra, C., Prati, M. V., et al. (2020). $\delta^{13}C$ signatures of organic aerosols: Measurement method evaluation and application in a source study. *Journal of Aerosol Science*, *145*, 105534. https://doi.org/10.1016/j.jaerosci.2020.105534

Zhang, Y. L., Huang, R. J., El Haddad, I., Ho, K. F., Cao, J. J., Han, Y., et al. (2015). Fossil vs. non-fossil sources of fine carbonaceous aerosols in four Chinese cities during the extreme winter haze episode of 2013. *Atmospheric Chemistry and Physics*, *15*(3), 1299–1312. https://doi.org/10.5194/acp-15-1299-2015

Zhao, Z., Cao, J., Shen, Z., Xu, B., Zhu, C., Chen, L. W. A., et al. (2013). Aerosol particles at a high-altitude site on the Southeast Tibetan Plateau, China: Implications for pollution transport from South Asia. *Journal of Geophysical Research: Atmospheres*, *118*(19), 11360–311375. https://doi.org/10.1002/jgrd.50599

Zhu, C.-S., Qu, Y., Huang, H., Chen, J., Dai, W.-T., Huang, R.-J., & Cao, J.-J. (2021). Black carbon and secondary brown carbon, the dominant light absorption and direct radiative forcing contributors of the atmospheric aerosols over the Tibetan Plateau. *Geophysical Research Letters*, *48*(11), e2021GL092524. https://doi.org/10.1029/2021GL092524

Zimnoch, M., Samek, L., Furman, L., Styszko, K., Skiba, A., Gorczyca, Z., et al. (2020). Application of natural carbon isotopes for emission source apportionment of carbonaceous particulate matter in urban atmosphere: A case study from Krakow, Southern Poland. *Sustainability*, *12*(14), 5777. https://doi.org/10.3390/su12145777

References From the Supporting Information

Aerts-Bijma, A. T., Paul, D., Dee, M. W., Palstra, S. W. L., & Meijer, H. A. J. (2020). An independent assessment of uncertainty for radiocarbon analysis with the new generation high-yield accelerator mass spectrometers. *Radiocarbon*, *63*(1), 1–22. https://doi.org/10.1017/RDC.2020.101

Bird, M. I., & Ascough, P. L. (2012). Isotopes in pyrogenic carbon: A review. *Organic Geochemistry*, *42*(12), 1529–1539. https://doi.org/10.1016/j.orggeochem.2010.09.005

Chen, P., Kang, S., Bai, J., Sillanpää, M., & Li, C. (2015). Yak dung combustion aerosols in the Tibetan Plateau: Chemical characteristics and influence on the local atmospheric environment. *Atmospheric Research*, *156*, 58–66. https://doi.org/10.1016/j.atmosres.2015.01.001

Chen, Y., Cai, W., Huang, G., Li, J., & Zhang, G. (2012). Stable carbon isotope of black carbon from typical emission sources in China. *Environmental Sciences*, *33*, 673–678. (in Chinese).

Clercq, M. L., Van Der Plicht, J., & Gröning, M. (2016). New ^{14}C reference materials with activities of 15 and 50 pMC. *Radiocarbon*, *40*(1), 295–297. https://doi.org/10.1017/S0033822200018178

Das, O., Wang, Y., & Hsieh, Y.-P. (2010). Chemical and carbon isotopic characteristics of ash and smoke derived from burning of C3 and C4 grasses. *Organic Geochemistry*, *41*(3), 263–269. https://doi.org/10.1016/j.orggeochem.2009.11.001

Drinovec, L., Močnik, G., Zotter, P., Prévôt, A. S. H., Ruckstuhl, C., Coz, E., et al. (2015). The "dual-spot" Aethalometer: An improved measurement of aerosol black carbon with real-time loading compensation. *Atmospheric Measurement Techniques*, *8*(5), 1965–1979. https://doi.org/10.5194/amt-8-1965-2015

Dusek, U., Monaco, M., Prokopiou, M., Gongriep, F., Hitzenberger, R., Meijer, H. A. J., & Röckmann, T. (2014). Evaluation of a two-step thermal method for separating organic and elemental carbon for radiocarbon analysis. *Atmospheric Measurement Techniques*, *7*(7), 1943–1955. https://doi.org/10.5194/amt-7-1943-2014

Gleason, J., & Kyser, T. (1984). Stable isotope compositions of gases and vegetation near naturally burning coal. *Nature*, *307*(5948), 254–257. https://doi.org/10.1038/307254a0

Guo, Z., Jiang, W., Chen, S., Sun, D., Shi, L., Zeng, G., & Rui, M. (2016). Stable isotopic compositions of elemental carbon in $PM_{1.1}$ in north suburb of Nanjing region, China. *Atmospheric Research*, *168*, 105–111. https://doi.org/10.1016/j.atmosres.2015.09.006

Hu, T., Cao, J., Lee, S., Ho, K., Li, X., Liu, S., & Chen, J. (2016). Physiochemical characteristics of indoor $PM_{2.5}$ with combustion of dried yak dung as biofuel in Tibetan Plateau, China. *Indoor and Built Environment*, *25*(5), 737–747. https://doi.org/10.1177/1420326X155865

Huang, L., Brook, J., Zhang, W., Li, S., Graham, L., Ernst, D., et al. (2006). Stable isotope measurements of carbon fractions (OC/EC) in airborne particulate: A new dimension for source characterization and apportionment. *Atmospheric Environment*, *40*(15), 2690–2705. https://doi.org/10.1016/j.atmosenv.2005.11.062

Jankowski, N., Schmidl, C., Marr, I. L., Bauer, H., & Puxbaum, H. (2008). Comparison of methods for the quantification of carbonate carbon in atmospheric PM_{10} aerosol samples. *Atmospheric Environment*, *42*(34), 8055–8064. https://doi.org/10.1016/j.atmosenv.2008.06.012

Kawashima, H., & Haneishi, Y. (2012). Effects of combustion emissions from the Eurasian continent in winter on seasonal $\delta^{13}C$ of elemental carbon in aerosols in Japan. *Atmospheric Environment*, *46*, 568–579. https://doi.org/10.1016/j.atmosenv.2011.05.015

Li, M. C., Liu, H. Y., Li, L., Yi, X., & Zhu, X. (2007). Carbon isotope composition of plants along altitudinal gradient and its relationship to environmental factors on the Qinghai-Tibet Plateau. *Polish Journal of Ecology*, *55*, 67–78.

Li, M. C., Liu, H. Y., Yi, X. F., & Li, L. X. (2006). Characterization of photosynthetic pathway of plant species growing in the eastern Tibetan plateau using stable carbon isotope composition. *Photosynthetica*, *44*(1), 102–108. https://doi.org/10.1007/s11099-005-0164-1

Liu, G., Li, M., & An, L. (2007). The environmental significance of stable carbon isotope composition of modern plant leaves in the northern Tibetan Plateau, China. *Arctic Antarctic and Alpine Research*, *39*(4), 678–681. https://doi.org/10.1657/1523-0430(07-505)[LIU-G]2.0.CO;2

Ni, H., Huang, R. J., Cao, J., Liu, W., Zhang, T., Wang, M., et al. (2018). Source apportionment of carbonaceous aerosols in Xi'an, China: Insights from a full year of measurements of radiocarbon and the stable isotope ^{13}C. *Atmospheric Chemistry and Physics*, *18*(22), 16363–16383. https://doi.org/10.5194/acp-18-16363-2018

NIOSH. (1999). Method 5040 Issue 3 (Interim): Elemental carbon (diesel exhaust). In *NIOSH manual of analytical methods*. National Institute of Occupational Safety and Health.

Ren, S.-J., & Yu, G.-R. (2011). Carbon isotope composition ($\delta^{13}C$) of C3 plants and water use efficiency in China. *Chinese Journal of Plant Ecology*, *35*(2), 119–124. (in Chinese). https://doi.org/10.3724/SP.J.1258.2011.00119

Schimmelmann, A., Qi, H., Coplen, T. B., Brand, W. A., Fong, J., Meier-Augenstein, W., et al. (2016). Organic reference materials for hydrogen, carbon, and nitrogen stable isotope-ratio measurements: Caffeines, n-Alkanes, fatty acid methyl esters, glycines, l-Valines, polyethylenes, and oils. *Analytical Chemistry*, *88*(8), 4294–4302. https://doi.org/10.1021/acs.analchem.5b04392

Stein, A. F., Draxler, R. R., Rolph, G. D., Stunder, B. J. B., Cohen, M. D., & Ngan, F. (2015). NOAA's HYSPLIT atmospheric transport and dispersion modeling system. *Bulletin of the American Meteorological Society*, *96*(12), 2059–2077. https://doi.org/10.1175/BAMS-D-14-00110.1

Tang, G. (2001). *$\delta^{13}C$ characteristics of carboniferous coal in North China and its paleo geographic implications*. Political Scholars Anthology of Peking University. Peking University. (in Chinese).

Wu, J., Kong, S., Wu, F., Cheng, Y., Zheng, S., Qin, S., et al. (2020). The moving of high emission for biomass burning in China: View from multi-year emission estimation and human-driven forces. *Environment International*, *142*, 105812. https://doi.org/10.1016/j.envint.2020.105812

Zenker, K., Vonwiller, M., Szidat, S., Calzolai, G., Giannoni, M., Bernardoni, V., et al. (2017). Evaluation and inter-comparison of oxygen-based OC-EC separation methods for radiocarbon analysis of ambient aerosol particle samples. *Atmosphere*, *8*(11), 226. https://doi.org/10.3390/atmos8110226

Zhang, Y. L., El-Haddad, I., Huang, R.-J., Ho, K.-F., Cao, J.-J., Han, Y., et al. (2018). Large contribution of fossil fuel derived secondary organic carbon to water soluble organic aerosols in winter haze in China. *Atmospheric Chemistry and Physics*, *18*(6), 4005–4017. https://doi.org/10.5194/acp-18-4005-2018

Zhang, Y. L., Li, J., Zhang, G., Zotter, P., Huang, R.-J., Tang, J.-H., et al. (2014). Radiocarbon-based source apportionment of carbonaceous aerosols at a regional background site on Hainan Island, South China. *Environmental Science & Technology*, *48*(5), 2651–2659. https://doi.org/10.1021/es4050852

Zhao, Z., Cao, J., Shen, Z., Huang, R.-J., Hu, T., Wang, P., et al. (2015). Chemical composition of $PM_{2.5}$ at a high-altitude regional background site over Northeast of Tibet Plateau. *Atmospheric Pollution Research*, *6*(5), 815–823. https://doi.org/10.5094/APR.2015.090